Journal of Anatomy

J. Anat. (2010) **217**, pp97–105 doi: 10.1111/j.1469-7580.2010.01248.x

Dynamic morphological changes in the skulls of mice mimicking human Apert syndrome resulting from gain-of-function mutation of FGFR2 (P253R)

Xiaolan Du, Tujun Weng, Qidi Sun, Nan Su, Zhi Chen, Huabing Qi, Ming Jin, Liangjun Yin, Qifen He and Lin Chen

State Key Laboratory of Trauma, Burns and Combined Injury, Center of Bone Metabolism and Repair, Trauma Center, Institute of Surgery Research, Daping Hospital, Third Military Medical University, Chongqing, China

Abstract

Apert syndrome is caused mainly by gain-of-function mutations of fibroblast growth factor receptor 2. We have generated a mouse model (*Fgfr2*$^{+/P253R)}$ mimicking human Apert syndrome resulting from fibroblast growth factor receptor 2 Pro253Arg mutation using the knock-in approach. This mouse model in general has the characteristic skull morphology similar to that in humans with Apert syndrome. To characterize the detailed changes of form in the overall skull and its major anatomic structures, euclidean distance matrix analysis was used to quantitatively compare the form and growth difference between the skulls of mutants and their wild-type controls. There were substantial morphological differences between the skulls of mutants and their controls at 4 and 8 weeks of age ($P < 0.01$). The mutants showed shortened skull dimensions along the rostrocaudal axis, especially in their face. The width of the frontal bone and the distance between the two orbits were broadened mediolaterally. The neurocrania were significantly increased along the dorsoventral axis and slightly increased along the mediolateral axis, and also had anteriorly displayed opisthion along the rostrocaudal axis. Compared with wild-type, the mutant mandible had an anteriorly displaced coronoid process and mandibular condyle along the rostrocaudal axis. We further found that there was catch-up growth in the nasal bone, maxilla, zygomatic bone and some regions of the mandible of the mutant skulls during the 4–8-week interval. The above-mentioned findings further validate the *Fgfr2*$^{+/P253R}$ mouse strain as a good model for human Apert syndrome. The changes in form characterized in this study will help to elucidate the mechanisms through which the Pro253Arg mutation in fibroblast growth factor receptor 2 affects craniofacial development and causes Apert syndrome.

Key words Apert syndrome; Euclidean distance matrix analysis; fibroblast growth factor receptor 2; mouse model; skull morphology.

Introduction

Apert syndrome (AS) is one of the severest forms of craniosynostosis (CS), and is caused mainly by either Ser252Trp (S252W) or Pro253Arg (P253R) mutation in fibroblast growth factor receptor 2 (FGFR2). Accounting for 4.5% of all cases of CS, AS is phenotypically characterized by syndactyly, premature fusion of coronal and less frequently other sutures (Kreiborg & Cohen, 1990; Cohen et al. 1992; Cohen & Kreiborg, 1996b). The distinctive craniofacial manifestations of AS include hyperacrobrachycephaly, shallow orbits with ocular proptosis, ocular hypertelorism, down-slanting palpebral fissures, depressed nasal bridge, and midface hypoplasia (Kreiborg et al. 1993, 1999; Cohen & Kreiborg, 1996a,b; Albuquerque & Cavalcanti, 2004; Pilet et al. 2007). Although there are a number of studies on the pathogenesis of human AS, our understanding of its molecular and cellular mechanisms is still incomplete. To explore the underlying mechanisms responsible for AS, and find appropriate cures for AS, we generated the mouse model (*Fgfr2*$^{+/P253R}$) mimicking human AS resulting from FGFR2 P253R mutation using the knock-in approach. In general, this mouse model shows gross skull phenotypes similar to

Correspondence
Lin Chen, State Key Laboratory of Trauma, Burns and Combined Injury, Center of Bone Metabolism and Repair, Trauma Center, Institute of Surgery Research, Daping Hospital, Third Military Medical University, Chongqing 400042, China. T: 86 23 68702991; F: 86 23 68702991; E: linchen70@163.com

Accepted for publication *10 May 2010*
Article published online *17 June 2010*

those in human AS, which include brachycephaly and underdeveloped midface (Yin et al. 2008).

The skull is an intricately developed structure composed of multiple bony components. Although mice have been validated to be good models for exploring the mechanisms underlying the normal and abnormal development of human skulls, the dramatic gross differences between human and mouse skulls prompted us to characterize the *Fgfr2*$^{+/P253R}$ mouse model quantitatively, and to evaluate whether it indeed shows precise parallels to the craniofacial phenotypes of patients with AS. Furthermore, skull development is a dynamic process, and the skull phenotype of humans with AS is age-related (Kreiborg et al. 1993), but so far there is very limited information about the dynamic changes in craniofacial morphology of human AS.

In this study, we quantitatively compared, using the form difference matrix (FDM) and the growth difference matrix (GDM) module of Euclidean distance matrix analysis (EDMA) approach (Richtsmeier & Lele, 1993; Richtsmeier et al. 2000, 2002), the dynamic morphological changes (between 4 and 8 weeks of age) in the overall skull and its major anatomic regions in the *Fgfr2*$^{+/P253R}$ mouse strain. Our quantitative data showed that this mouse model had multiple skull abnormalities with obvious brachycephaly, shortened nasal bone, ocular hypertelorism, underdeveloped midface and malocclusion that were very similar to the skull abnormalities of humans with AS. Interestingly, we also found that there was catch-up growth in some regions of the mutant skulls between 4 and 8 weeks. Our data further validate the application of this mouse model to explore the pathogenesis and therapeutic measures for human AS.

Materials and methods

Preparation of skeletons and collection of landmark data

Fgfr2$^{+/P253R\text{-}neo}$ mice and EIIa-Cre mice were kindly provided by Dr Chuxia Deng of NIDDK, and permission to use the EIIa-Cre mice was provided by Dr Westphal. Both EIIa-Cre mice and *Fgfr2*$^{+/P253R\text{-}neo}$ mice were inbred to a C57BL/6J background by mating with C57BL/6J mice for 10 generations. *Fgfr2*$^{+/P253R}$ mice were generated by crossing male offspring of *Fgfr2*$^{+/P253R\text{-}neo}$ and female offspring of EIIa-Cre mice. All procedures were approved by the Institutional Animal Care and Use Committee of Daping Hospital. Mice were genotyped as described. About 37% of the mutant mice died before 8 weeks of age. Four-week-old and 8-week-old *Fgfr2*$^{+/P253R}$ mice and wild-type (WT) mice from the same litter were used. After being killed, the mouse carcasses were skinned and gutted, and finally cleaned by surgical dissection and ants as described previously (Yin et al. 2008).

According to Richtsmeier's method (Richtsmeier et al. 2000, 2002; Hill et al. 2007), three-dimensional coordinate locations of 28 biologically relevant landmarks located on the crania (Fig. 1A–C) and 11 biologically relevant landmarks located on the left mandible (Fig. 3A) were recorded from 12 skulls of 4-week-old *Fgfr2*$^{+/P253R}$ mutant and WT mice, as well as 12 skulls of 8-week-old *Fgfr2*$^{+/P253R}$ and WT mice using a MarVision PMC 800 measuring machine (Carl Mahr Holding GmbH, Germany).

Morphometric methods

The coordinate data collected were analyzed using EDMA to calculate the differences in form and growth between mutant mice and their WT controls. EDMA is a method for quantitative analyses of form and growth characteristics in the geometric morphology (Richtsmeier & Lele, 1990; Lele & Richtsmeier, 1995). In EDMA, 3D landmark coordinate data are converted to a matrix of all possible linear distances between unique pairs of landmarks. There are K(K−1)/2 linear distances in the matrix when K landmarks are given for a specimen (A), so the form of a specimen can be quantitatively described by the matrix of all inter-landmark linear distances of the specimen in EDMA. The matrix is called the form matrix [FM$(A)_{ij}$ and i, j = 1…K] of the specimen (A). The form difference matrix (FDM) is used to calculate statistically whether the given two samples (A and B) are significantly different in shape by comparing the mean forms of two samples (A and B). It is defined as follows:

$$\mathrm{FDM}\,(\mathrm{A},\ \mathrm{B})_{ij} = \frac{\mathrm{FM}\,(\mathrm{A})_{ij}}{\mathrm{FM}\,(\mathrm{B})_{ij}}$$

The growth matrix (GM) for the specimen (A) during the development interval (age 1 and 2) is defined as follows:

$$\mathrm{GM}\,(\mathrm{A}_1 \rightarrow \mathrm{A}_2)_{ij} == \frac{\mathrm{FM}\,(\mathrm{A}_2)_{ij}}{\mathrm{FM}\,(\mathrm{A}_1)_{ij}}$$

The growth difference matrix (GDM) is used to analyze the difference in the growth rate between two samples (A and B) during a specific developmental period (age 1 and 2). It is defined as follows:

$$\mathrm{GDM}\,(\mathrm{A}_1 \rightarrow \mathrm{A}_2, \mathrm{B}_1 \rightarrow \mathrm{B}_2)_{ij} = \frac{\mathrm{GM}\,(\mathrm{A}_1 \rightarrow \mathrm{A}_2)_{ij}}{\mathrm{GM}\,(\mathrm{B}_1 \rightarrow \mathrm{B}_2)_{ij}} = \frac{\mathrm{FM}\,(\mathrm{A}_2)_{ij}/\mathrm{FM}\,(\mathrm{A}_1)_{ij}}{\mathrm{FM}\,(\mathrm{B}_2)_{ij}/\mathrm{FM}\,(\mathrm{B}_1)_{ij}}$$

Statistical significances for the form and growth differences in the inter-landmark linear distances are evaluated by using confidence intervals (α = 0.05) calculated by a nonparametric bootstrap method (1000 bootstrapped steps). If all the ratios of the matrix in FDM (GDM) equal 1 or a constant, the shape (growth) of two samples is considered identical, or the shape (growth) of two samples are the same but their sizes are different. If the ratios of the FDM (GDM) are heterogeneous, a difference in shape (growth) is indicated. When the range of the FDM (GDM) is 0.95–1.05, it indicates that ≤5% changes of an inter-landmark distance in form (growth) are present. Values <0.95 or >1.05 indicate that there are >5% decreases or increases of an inter-landmark distance in form (growth) between two compared samples, respectively.

The 3D data of the crania [landmarks K = 28, K(K−1)/2 = 378 linear distances, Fig. 1A–C] and the left mandible [landmarks K = 11, K(K−1)/2 = 55 linear distances, Fig. 2A] (Richtsmeier et al. 2000; Hill et al. 2007) of 4- and 8-week-old *Fgfr2*$^{+/P253R}$ mice and their littermate WT mice were analyzed using WinE-DMA software downloaded from http://getahead.psu.edu. The patterns of form and growth difference between *Fgfr2*$^{+/P253R}$ and WT are described by specific landmarks and the linear distances by naming the landmarks that serve as endpoints of

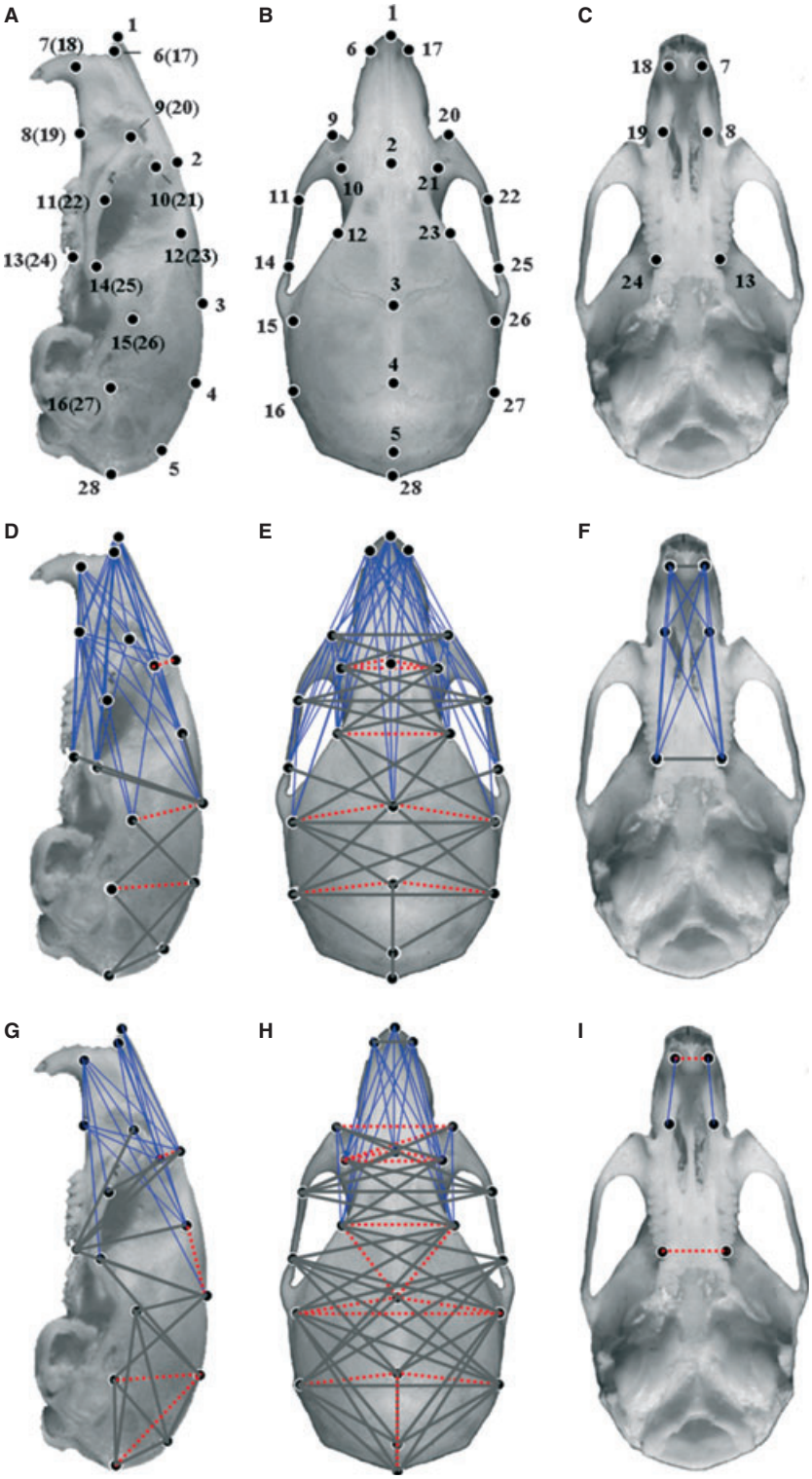

Fig. 1 Normal mouse cranium with locations of landmarks used to analyze the morphology differences between Mu mice and littermate WT mice at 4 and 8 weeks. Lateral view of the cranium (A,D,G), superior view of the cranium (B,E,H), bottom view of cranium (C,F,I). Normal mouse cranium with locations of 27 landmarks (A–C). Form difference analysis between Mu and WT mice at 4 weeks (D–F). Form difference analysis between Mu and WT mice at 8 weeks (G–I). Thin blue lines show those linear distances that showed a decrease of over 30% in Mu mice. Thick grey lines indicate that some of those linear distances had a <5% difference between Mu and WT mice. Broken red lines show linear distances with a >5% increase in Mu mice. Mu, *Fgfr2*$^{+/P253R}$; WT, wild-type.

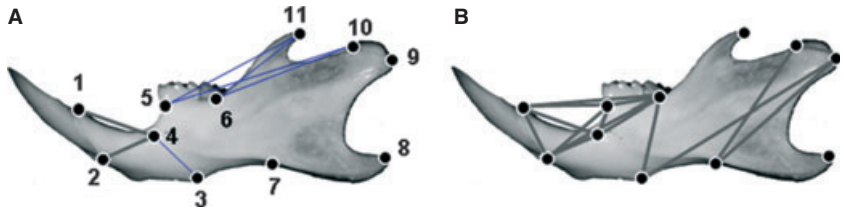

Fig. 2 Normal left mouse mandible with locations of landmarks used in this study. Form difference analysis between Mu and WT mice at 4 weeks (A) and 8 weeks (B). Thin blue lines show linear distances that decreased by over 30% in Mu mice. Thick grey lines represent some of the linear distances with a <5% difference between Mu and WT mice. Mu, *Fgfr2*$^{+/P253R}$; WT, wild-type.

the linear distance (e.g. the linear distance between landmark 1 and landmark 2 is described as 'landmarks 1 and 2').

Results

The form characteristics of the skulls of *Fgfr2*$^{+/P253R}$ mice

FDM analysis was used to evaluate the morphology of the crania of 4- and 8-week-old *Fgfr2*$^{+/P253R}$ mice and their littermate controls. Dramatic changes in the overall cranium shapes of 4- and 8-week-old mutants were revealed ($P < 0.01$). For 4-week-old *Fgfr2*$^{+/P253R}$ mice, 90% linear distances were shortened by over 5%, 21% linear distances showed a >30% decrease (marked by thin blue lines in Fig. 1D–F), 8% linear distances exhibited a <5% change (marked by thick grey lines in Fig. 1D–F), and only 2% linear distances (marked by broken red lines in Fig. 1D–F) displayed an increase of over 5%. For 8-week-old *Fgfr2*$^{+/P253R}$ mice, 77% linear distances showed a decrease of over 5%, 11% linear distances (marked by thin blue lines in Fig. 1G–I) had a decrease of over 30%, 19% linear distances (marked by thick grey lines in Fig. 1G–I) exhibited a <5% change, and 4% linear distances (marked by broken red lines in Fig. 1G–I) showed a >5% increase in *Fgfr2*$^{+/P253R}$ mouse crania.

Overall, for the mutant skulls, the linear distances oriented along the rostrocaudal (RC) direction were shortened. The length of the mutant skulls (landmarks 1 and 28) was shortened by 22.6% at 4 weeks and 17.8% at 8 weeks. The significantly shortened distances were mainly located in the anterior regions of the mutant crania. Some linear distances oriented along the mediolateral (ML) and dorsoventral (DV) direction were increased. However, there were differences in the magnitudes of malformation between *Fgfr2*$^{+/P253R}$ mice at 4 and 8 weeks. To further characterize the detailed differences in the crania between *Fgfr2*$^{+/P253R}$ and WT mice, we analyzed the changes in the face and neurocranium as follows.

Face

At the 4-week stage, the faces of *Fgfr2*$^{+/P253R}$ mice were significantly shortened along the RC axis (Table 1). The nasal bone (landmarks 1 and 2) was the most significantly shortened region, showing a 50.2% decrease in length. The frontal bone (landmarks 2 and 3) exhibited a 20.4% decrease. The frontal processes of the maxilla (landmarks 9 and 10, 20 and 21) in *Fgfr2*$^{+/P253R}$ mice were also shortened by 41.7% on average, and the premaxilla (landmarks 7 and 8, 18 and 19) and maxilla length (landmarks 8 and 13, 19 and 24) were decreased by 35.5 and 30.7% on average, respectively. The zygomatic bone (landmarks 11 and 14, 22 and 25) was substantially shortened in mutants by 32.1% on average. We then observed the form changes in the face along the ML direction. The distance between two orbits (landmarks 10 and 21) was increased by 17.6%, and the width of the frontal bone (landmarks 12 and 23) was increased by 11.7% in *Fgfr2*$^{+/P253R}$ mice. The linear distances of the paired center of alveolar ridge over maxillary incisor (landmarks 7 and 18), the paired frontal processes of the maxilla (landmarks 9 and 20) and the paired anterior zygoma (landmarks 11 and 22) exhibited a <5% change. The width of the posterior palate (landmarks 13 and 24) also had a <5% change. The width of the nasal bone (landmarks 6 and 17) and the anterior palate (landmarks 8 and 19) along the ML direction was decreased by 5.2 and 7.4%, respectively. The linear distance of the paired posterior zygoma (landmarks 14 and 25) along ML direction was decreased by 6.5%.

At the 8-week stage, the face dimensions along the RC axis of *Fgfr2*$^{+/P253R}$ mice were less significantly shortened than those in 4-week-old mutants (Table 1). Compared with WT littermate controls, the mutants showed a 41.1 and 18.6% decrease in the length of their nasal bone (landmarks 1 and 2) and frontal bone (landmarks 2 and 3), respectively. The 8-week-old mutants still exhibited severely shortened frontal processes of the maxilla (landmarks 9 and 10, 20 and 21) as evidenced by a 41.5% decrease on average. The premaxilla length (landmarks 7 and 8, 18 and 19) also displayed a 33.1% reduction on average in comparison with WT controls. Compared with 4-week-old *Fgfr2*$^{+/P253R}$ mice, the magnitude of the shortening of the length of maxilla (landmarks 8 and 13, 19 and 24) and zygomatic bone (landmarks 11 and 14, 22 and 25) of 8-week-old *Fgfr2*$^{+/P253R}$ mice was substantially alleviated; there was only a 17.6 and 23.5% decrease on average in their maxilla and zygomatic bone length,

Table 1 The local linear distances ratios of the form and growth difference matrices for the comparison of face and neurocranium of Mu and Wt at 4 and 8 weeks.

Landmarks	FDM Mu-to-MT Comparison (4 weeks)	FDM Mu-to-MT Comparison (8 weeks)	GDM Mu (8 weeks)-to-Mu (4 weeks) comparison WT (8 weeks)- to- WT (4 weeks)
1 and 2	0.498	0.589	1.191
2 and 3	0.796	0.814	1.069
9 and 10 (20 and 21)	0.583	0.585	1.021
7 and 8 (18 and 19)	0.645	0.669	1.033
8 and 13 (19 and 24)	0.693	0.824	1.173
11 and 14 (22 and 25)	0.679	0.765	1.157
10 and 21	1.176	1.181	1.005
12 and 23	1.117	1.139	1.020
7 and 18	1.010	1.057	1.042
9 and 20	1.038	1.070	1.031
11 and 22	0.958	0.990	1.044
13 and 24	1.045	1.079	1.032
6 and 17	0.948	0.988	1.029
8 and 19	0.926	0.943	1.017
14 and 25	0.935	0.947	1.047
2 and 28	0.839	0.896	1.069
3 and 4	0.832	0.838	1.002
4 and 5	1.024	1.038	1.029
5 and 28	0.988	1.034	1.048
15 and 16 (26 and 27)	0.908	0.926	1.064
5 and 13 (5 and 24)	0.879	0.864	0.976
28 and 13 (28 and 24)	0.834	0.850	1.020
15 and 26	1.009	1.052	1.015
16 and 27	1.002	1.022	1.019
3 and 15 (3 and 26)	1.065	1.065	0.993
4 and 16 (4 and 27)	1.075	1.083	1.013

Mu, *Fgfr2*$^{+/P253R}$; WT, wild-type.

respectively. For 8-week-old *Fgfr2*$^{+/P253R}$ mice, along the ML direction, the distance between two orbits (landmarks 10 and 21) was increased by 18.1%, and the frontal bone width (landmarks 12 and 23) by 13.9%. The distance of the paired center of alveolar ridge over maxillary incisor (landmarks 7 and 18) and the paired frontal processes of the maxilla (landmarks 9 and 20) was increased by 5.7 and 7.0%, respectively. The width of the posterior palate (landmarks 13 and 24) was increased by 7.9%, and the width of the nasal bone (landmarks 6 and 17) and the distance of the paired frontal zygoma (landmarks 11 and 22) had a <5% difference between *Fgfr2*$^{+/P253R}$ and WT mice. The width of the anterior palate (landmarks 8 and 19) and the distance of the paired posterior zygoma (landmarks 14 and 25) along the ML direction were decreased by 5.7 and 5.3%, respectively.

The significantly reduced length of the nasal bone, maxillae and zygoma, as well as the ocular hypertelorism and increased width of frontal bone in *Fgfr2*$^{+/P253R}$ mice at both the 4- and the 8-week stages closely paralleled the characteristic facial morphology of humans with AS, including shortened nasal bone, midface hypoplasia and shallow orbits (Cohen & Kreiborg, 1996a; Albuquerque & Cavalcanti, 2004).

Neurocranium

In 4-week-old *Fgfr2*$^{+/P253R}$ mice, compared with WT littermates, the length of the neurocrania (landmarks 2 and 28) was decreased by 16.1% along the RC axis. The dimension of the parietal bone (landmarks 3 and 4) was decreased by 16.8%. The dimension of the interparietal bone (landmarks 4 and 5) and the occiput (landmarks 5 and 28) showed a <5% change. The linear distance between landmark 15 and 16 and between landmark 26 and 27 displayed an average decrease of 9.2%. The linear distances between the intersection of interparietal and occipital bones at the midline and the posterior palate (landmarks 5 and 13, 5 and 24) showed an average decrease of 12.1%. The linear distances between the opisthion and the posterior palate (landmarks 28 and 13, 28 and 24) exhibited an average decrease of 16.6%. These results indicated that the opisthion of *Fgfr2*$^{+/P253R}$ mouse skull was displaced anteriorly along the RC axis. In ML direction, the neurocranium widths (landmarks 15 and 26, 16 and 27) had a <5% change when compared with WT controls. The linear distance of landmarks 3 and 15 (3 and 26) and landmarks 4 and 16 (4 and 27) were increased on average by 6.5 and 7.5%, respectively. These data indicated that the cranium height of *Fgfr2*$^{+/P253R}$

mouse along their dorsoventral (DV) axis was increased (Table 1).

In 8-week-old *Fgfr2*$^{+/P253R}$ mice, the neurocrania were still reduced along the RC axis and slightly increased along the ML axis. The neurocranium length (landmarks 2 and 28) showed a 10.4% decrease. The parietal bone (landmarks 3 and 4) was reduced by 16.2%, and the length of the interparietal bone (landmarks 4 and 5) and the occiput (landmarks 5 and 28) still showed a <5% change. The linear distance of landmarks 15 and 16 (26 and 27) showed an average decrease of 7.4%. The linear distances between the intersection of interparietal and occipital bones at the midline and the posterior palate (landmarks 5 and 13, 5 and 24) showed an average decrease of 13.6%. The linear distances between the opisthion and the posterior palate (landmarks 28 and 13, 28 and 24) exhibited an average decrease of 15.0%. There was a 5.2% increase in the anterior neurocrania (landmarks 15 and 26), compared with an increase of <5% in the width of the posterior portion (landmarks 16 and 27) along the ML axis. The distances of landmarks 3 and 15 (3 and 26) and landmarks 4 and 16 (4 and 27) were increased on average by 6.5 and 8.3%, respectively (Table 1).

All these data showed that *Fgfr2*$^{+/P253R}$ mice at both the 4- and 8-weeks stage had a rostrocaudally decreased cranial length, increased cranium height along the DV axis, slightly increased along the mediolateral (ML) and anteriorly displayed opisthion along the RC axis, which closely resembled the brachycephaly and flat occiput found in humans with AS (Cohen & Kreiborg, 1994, 1996a).

Table 2 The local linear distances ratios of the form and growth difference matrices for the comparison mandible of Mu and Wt at 4 and 8 weeks.

Landmarks	FDM Mu-to-MT Comparison (4 weeks)	FDM Mu-to-MT Comparison (8 weeks)	GDM Mu (8 weeks)-to-Mu (4 weeks) comparison WT (8 weeks)- to-WT (4 weeks)
1 and 2	0.873	0.951	1.089
1 and 4	1.036	1.021	0.985
1 and 5	0.941	1.017	1.081
1 and 6	0.894	1.014	1.134
2 and 4	1.027	1.012	0.986
2 and 5	0.893	0.985	1.103
2 and 6	0.877	1.001	1.135
3 and 4	0.695	0.832	1.197
3 and 6	0.883	0.971	1.100
4 and 5	0.855	0.963	1.133
4 and 6	0.849	0.974	1.145
5 and 6	0.878	1.001	1.140
3 and 9	0.841	0.955	1.193
7 and 9	0.805	0.992	1.136
7 and 8	0.874	0.902	1.032
4 and 10	0.775	0.910	1.182
7 and 10	0.829	0.953	1.141
9 and 10	0.875	0.980	1.120
5 and 10	0.697	0.886	1.246
5 and 11	0.689	0.865	1.250
6 and 10	0.670	0.843	1.288
6 and 11	0.658	0.828	1.259
8 and 11	0.826	0.857	1.038

Mu, *Fgfr2*$^{+/P253R}$; WT, wild-type.

Mandible

Using the left mandibular landmarks, we tested the null hypothesis of similarity in mandible shapes between *Fgfr2*$^{+/P253R}$ mice and WT littermate controls. The overall shapes of the mandible of both 4- and 8-week-old *Fgfr2*$^{+/P253R}$ mice differed from their normal controls ($P < 0.05$). At 4 weeks, only two dimensions (landmarks 1 and 4, 2 and 4) showed a <5% difference between *Fgfr2*$^{+/P253R}$ mice and WT controls (marked by thick grey lines in Fig. 2A). The other 53 distances were shortened by over 5% in mutants. Several dimensions (landmarks 3 and 4, 5 and 10, 5 and 11, 6 and 10, 6 and 11) in mutants showed a 30–35% reduction (marked by thin blue lines in Fig. 2A). At 8 weeks, the shortening magnitudes of the mutant mandible were markedly alleviated. Fifteen linear distances exhibited no significant differences between WT and mutants (marked by thick grey lines in Fig. 2B). Ten of these 15 dimensions were concentrated either in the region composed of the incisor alveolar rim, mandibular foramen and molar (landmarks 1, 2, 4, 5, 6), three linear distances were located in the triangular area formed between the mandibular condyle (landmarks 9 and 10) and superior-most point on the inferior border of mandibular ramus (landmark 7). The remaining 40 distances were still shortened in mutants but to a milder degree. For example, the distances between landmarks 6 and 10 and 6 and 11 were still reduced by 15.7 and 17.2%, respectively (Table 2).

The growth characteristics of the skulls of *Fgfr2*$^{+/P253R}$ mice between 4 and 8 weeks

Craniofacial development is a dynamic process, during which the growths of individual craniofacial components need to be coordinated. The craniofacial malformation in AS indicates that there may be differential developmental dynamics among distinct anatomic regions. So far there are few analyses of the growth rates of the skulls of mouse models mimicking human AS (Chen et al. 2003; Wang et al. 2005). We thus analyzed, using GDM, the dynamic form changes in the overall crania and its major anatomic structures in both mutants and their WT controls during the developmental interval between 4 and 8 weeks.

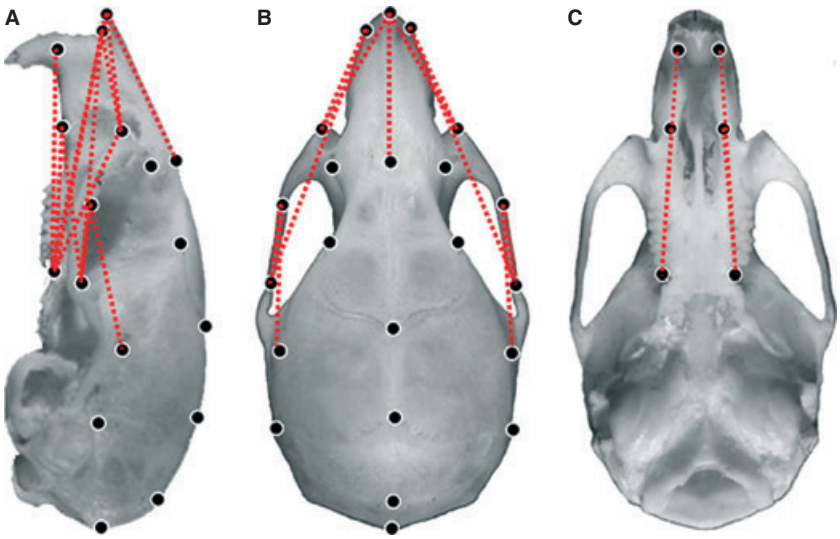

Fig. 3 Normal mouse cranium with locations of landmarks used to analyze the growth differences of Mu (8 weeks)-to-Mu (4 weeks) comparison WT (8 weeks)-to-WT (4 weeks). Lateral view of the cranium (A), superior view of the cranium (B), bottom view of the cranium (C). Broken red lines show linear distances with an increased growth of over 15% in the Mu mice. Mu, *Fgfr2*$^{+/P253R}$; WT, wild-type.

No significant difference in the global growth of the crania between Mu and WT was found during the 4–8-week period ($P = 0.443$). However, confidence interval testing ($0.95 \leq \alpha \leq 1.05$) revealed significantly different growth in some structures of the crania. In *Fgfr2*$^{+/P253R}$ mice, 53% dimensions showed a >5% increased growth, 7% dimensions in mutants showed an increase in growth of over 15% (marked by red broken lines in Fig. 3), and 47% dimensions had <5% growth changes during the 4–8-week period.

Face

Compared with that of WT littermates, the nasal (landmarks 1 and 2) and frontal bone (landmarks 2 and 3) of *Fgfr2*$^{+/P253R}$ mice had a 19.1 and 6.9% increased growth in length, respectively. The frontal processes of the maxilla (landmarks 9 and 10, 20 and 21) and premaxilla (landmarks 7 and 8, 18 and 19) both had a <5% growth change on average. The length of the maxilla (landmarks 8 and 13, 19 and 24) and zygomatic bone (landmarks 11 and 14, 22 and 25) showed an increase in growth of 17.3 and 15.7% average, respectively. Along the ML direction, linear distances between multiple paired points (landmarks 6 and 17, 7 and 18, 8 and 19, 9 and 20, 10 and 21, 12 and 23, 13 and 24, 11 and 22, 14 and 25) had a <5% growth change (Table 1).

Neurocranium

Compared with WT littermates, the dimension of the length of the neurocranium along the RC axis (landmarks 2 and 28) had a 6.9% increased growth. The parietal bone (landmarks 3 and 4), the interparietal bone (landmarks 4 and 5) and the occiput (landmarks 5 and 28) had <5% growth in *Fgfr2*$^{+/P253R}$ mice along RC axis. The dimension between landmarks 15 and 16 (landmarks 26 and 27) had a 6.4% increased growth. The linear distance between the intersection of interparietal and occipital bone at the midline and the posterior palate (landmarks 5 and 13, 5 and 24) had a <5% growth. The linear distances between the opisthion and the posterior palate (landmarks 28 and 13, 28 and 24) showed an average increased growth of 6.4%. The neurocranium widths (landmarks 15 and 26, 16 and 27) of *Fgfr2*$^{+/P253R}$ mice and several dimensions of the vault [landmarks 3 and 15 (3 and 26), 4 and 16 (4 and 27)] had a <5% growth change during the 4–8-week interval (Fig. 3, Table 1).

Mandible

GDM analyses of the mandible were carried out for *Fgfr2*$^{+/P253R}$ and WT mice during the 4–8-week interval using 11 landmarks (55 linear distances) of the left mandible. There were no significant differences in the global growth of the mandibles between Mu and WT during the 4–8-week period ($P = 0.369$). Four of the 55 dimensions showed a <5% difference in growth between *Fgfr2*$^{+/P253R}$ and WT mice (marked by thick grey lines in Fig. 4). The other 51 dimensions in *Fgfr2*$^{+/P253R}$ mice exhibited an increase of over 5%. The dimensions between landmarks 3 and 4, 4 and 10, 5 and 10, 5 and 11, 6 and 10, 6 and 11 had an increased growth of over 15% (marked by broken red lines in Fig. 4), indicating that during the 4–8-week period these regions in the mandible of *Fgfr2*$^{+/P253R}$ mice developed faster than the corresponding regions in WT mice (Table 2).

Discussion

Although there are several studies on the craniofacial phenotype of mouse models for Apert syndrome and its underlying mechanisms (Chen et al. 2003; Wang et al. 2005; Yin et al. 2008; Holmes et al. 2009), there are still few quantitative analyses of the craniofacial morphology of these

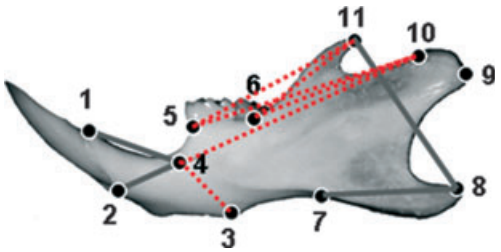

Fig. 4 Normal left mandible with locations of landmarks used to analyze the growth differences of Mu (8 weeks)-to-Mu (4 weeks) comparison WT (8 weeks)-to-WT (4 weeks). Thick grey lines represent linear distances with a growth difference of <5% between mutants and WT mice during the 4- and 8-week interval. Broken red lines show linear distances that had an increased growth of over 15% in the Mu mice during 4–8-week interval. Mu, *Fgfr2*$^{+/P253R}$; WT, wild-type.

models (Wang et al. 2005; Yin et al. 2008). In this study, using FDM and GDM analyses, we quantitatively characterized the form and growth changes in the overall skulls and its major anatomic regions of *Fgfr2*$^{+/P253R}$ mice along AC, ML and DV axis. Besides the expected brachycephaly of *Fgfr2*$^{+/P253R}$ mice, multiple individual anatomic regions of the skulls also displayed significant form changes with differential magnitudes at both 4 and 8 weeks. Along AC axis, the face (nasal and frontal bone, premaxilla, maxilla and zygoma) was more remarkably shortened than the neurocrania, which may be responsible for the malocclusion in mutants. Along ML axis, the distance between two orbits and the frontal bone width were significantly broadened in mutants, while the width of the neurocranium was slightly increased at 8 weeks. The mutant neurocrania had increased dimensions along the DV axis and anteriorly displayed occiput along RC direction at both 4 and 8 weeks. All these changes in mutant skulls make *Fgfr2*$^{+/P253R}$ mice phenotypically similar to humans with AS (Cohen & Kreiborg, 1996a; Kreiborg et al. 1999; Pilet et al. 2007). The reasons for the increased width of the frontal bone and the increased lengths of multiple dimensions along the ML and DV axes in neurocrania are not clear at present. Further studies are needed to observe whether these changes are compensations for the shortened length along RC axis, or are caused directly by the mutation itself.

Craniofacial development is a dynamic process. The dysmorphology of the skulls of humans with AS is also age-dependent (Kreiborg et al. 1993). In previous studies of the mouse models for AS, no detailed analyses of the dynamic changes of the mutant skulls were carried out (Chen et al. 2003; Wang et al. 2005). In this study, using GDM analyses, we found that there were catch-up growths in some regions of the mutant skulls during the 4–8-week interval. Interestingly, the catch-up growth in the cranial vault occurred mainly in some anatomic regions along the RC direction. The nasal bone, maxilla and zygomatic bone showed obvious catch-up growth along RC axis, although they were still shorter than that in WT mice at 8 weeks. The reasons for the catch-up development in these regions are not clear so far. As these bones are not likely related to the volume of neurocrania directly, their catch-up development may not be a compensation for the changed neurocranial volume, and may be caused by the mutation itself. In contrast, several regions that are more likely related to cranial volume including frontal bone (landmarks 2 and 3), parietal (landmarks 3 and 4) and interparietal bone (landmarks 4 and 5) in *Fgfr2*$^{+/P253R}$ mice did not show significant catch-up growth along RC axis. The lengths of frontal and parietal bone along RC axis were significantly shortened in mutants at both 4 and 8 weeks. The persistently shortened crania along the AC axis may be related to the premature fusion of coronal sutures, which happened in all cases. The major dimensions along the ML and DV axes of the mutant vault were larger than or at least similar to that in wild-type controls, which may compensate the restrained development of the skulls along AC axis.

As part of the skull, a number of studies have analyzed the changes of the mandibles in humans with AS (Kreiborg & Cohen, 1992; Kreiborg et al. 1999). Although Kreiborg et al. (1999) reported that mandible of individuals with AS are not small, but the mandibular prognathism or malocclusion is a 100% penetrant phenotype found in patients carrying FGFR2 P253R mutation, which indicates the potential maldevelopment of the mandible. Wang et al. (2005) found very small mandible with a dysmorphic angular process in *Fgfr2*$^{+/S252W}$ mice. In this study, we found globally reduced mandibular dimensions in *Fgfr2*$^{+/P253R}$ mice, but the reductions of mandible were much milder than those of the crania along the RC axis. Our further analyses revealed that the reductions were mainly located in the posterior regions of the mandible (the coronoid process, mandibular condyle and mandibular angle) along the RC axis, but the magnitude of shortening was alleviated at 8 weeks.

We further analyzed the dynamic morphological changes in the mandible using GDM, which also revealed catch-up growth in multiple dimensions of the mandible during the 4–8-week interval. The linear distances between coronoid process and molar showed significant catch-up growth along the RC axis. At 8 weeks, more dimensions in the front portion of the mutant mandible were similar to those in the WT mandible.

These dynamic skull form changes found in *Fgfr2*$^{+/P253R}$ mice need to be confirmed in the future in corresponding patients. In the surgical treatment of patients with craniosynostosis, the development dynamics of the maxilla and mandible have to be considered (Fearon, 2005), and the potential clinical significance of our findings for the treatment of patients with AS need to be studied further. The craniofacial anomalies found in humans with AS and our *Fgfr2*$^{+/P253R}$ mice indicate that dysregulated development existed in both facial bone and cranial vault. The role of

FGFs/FGFRs in cranial suture development has been investigated in a variety of studies, but the function of FGFRs in the normal development and diseases of facial bone is still relatively elusive (Szabo-Rogers et al. 2008). Whether the abnormal facial development in *Fgfr2*$^{+/P253R}$ mice is caused directly by the abnormal FGFR2 activity in those facial structures and/or is secondary to the abnormal cranial vault development needs to be studied in the future. In this cross-sectional study, some mutants died before analyses, indicating the phenotype variations in mutants, which may introduce some bias into the results. Serial morphology analyses of the individual living mice using *in vivo* micro-CT may solve this problem in the future.

In summary, using both FDM and GDM analyses, we quantitatively evaluated the craniofacial skeleton phenotypes of the mutants carrying FGFR2 P253R mutation. Besides the characteristic form changes in mutant skulls and its major anatomic regions including mandible, we found that some anatomical regions of the skulls of *Fgfr2*$^{+/P253R}$ mice had catch-up growth. These findings further validate the using of the mutant mice carrying FGFR2 P253R mutation to study the mechanism and therapeutic approaches of AS, and provide some new clues for the future analyses of skull phenotypes and clinical management of AS.

Acknowledgements

We thank Professor J. T. Richtsmeier for providing us with EDMA software. This work is supported by the Major State Basic Research Development Program of China (No. 2005CB522604) and the National Natural Science Foundation of China (No. 30530410, 30971607).

References

Albuquerque MA, Cavalcanti MG (2004) Computed tomography assessment of Apert syndrome. *Pesqui Odontol Bras* **18**, 35–39.

Chen L, Li D, Li C, et al. (2003) A Ser252Trp [corrected] substitution in mouse fibroblast growth factor receptor 2 (Fgfr2) results in craniosynostosis. *Bone* **33**, 169–178.

Cohen MM Jr, Kreiborg S (1994) Cranial size and configuration in the Apert syndrome. *J Craniofac Genet Dev Biol* **14**, 153–162.

Cohen MM Jr, Kreiborg S (1996a) A clinical study of the craniofacial features in Apert syndrome. *Int J Oral Maxillofac Surg* **25**, 45–53.

Cohen MM Jr, Kreiborg S (1996b) Suture formation, premature sutural fusion, and suture default zones in Apert syndrome. *Am J Med Genet* **62**, 339–344.

Cohen MM Jr, Kreiborg S, Lammer EJ, et al. (1992) Birth prevalence study of the Apert syndrome. *Am J Med Genet* **42**, 655–659.

Fearon JA (2005) Halo distraction of the Le Fort III in syndromic craniosynostosis: a long-term assessment. *Plast Reconstr Surg* **115**, 1524–1536.

Hill CA, Reeves RH, Richtsmeier JT (2007) Effects of aneuploidy on skull growth in a mouse model of Down syndrome. *J Anat* **210**, 394–405.

Holmes G, Rothschild G, Roy UB, et al. (2009) Early onset of craniosynostosis in an Apert mouse model reveals critical features of this pathology. *Dev Biol* **328**, 273–284.

Kreiborg S, Cohen MM Jr (1990) Characteristics of the infant Apert skull and its subsequent development. *J Craniofac Genet Dev Biol* **10**, 399–410.

Kreiborg S, Cohen MM Jr (1992) The oral manifestations of Apert syndrome. *J Craniofac Genet Dev Biol* **12**, 8.

Kreiborg S, Marsh JL, Cohen MM Jr, et al. (1993) Comparative three-dimensional analysis of CT-scans of the calvaria and cranial base in Apert and Crouzon syndromes. *J Craniomaxillofac Surg* **21**, 181–188.

Kreiborg S, Aduss H, Cohen MM Jr (1999) Cephalometric study of the Apert syndrome in adolescence and adulthood. *J Craniofac Genet Dev Biol* **19**, 1–11.

Lele S, Richtsmeier JT (1995) Euclidean distance matrix analysis: confidence intervals for form and growth differences. *Am J Phys Anthropol* **98**, 73–86.

Pilet B, Vanhoenacker FM, De Beuckeleer L, et al. (2007) Craniofacial dysmorphism in Apert syndrome. *JBR-BTR* **90**, 202–203.

Richtsmeier JT, Lele S (1990) Analysis of craniofacial growth in Crouzon syndrome using landmark data. *J Craniofac Genet Dev Biol* **10**, 39–62.

Richtsmeier JT, Lele S (1993) A coordinate-free approach to the analysis of growth patterns: models and theoretical considerations. *Biol Rev Camb Philos Soc* **68**, 381–411.

Richtsmeier JT, Baxter LL, Reeves RH (2000) Parallels of craniofacial maldevelopment in Down syndrome and Ts65Dn mice. *Dev Dyn* **217**, 137–145.

Richtsmeier JT, Zumwalt A, Carlson EJ, et al. (2002) Craniofacial phenotypes in segmentally trisomic mouse models for Down syndrome. *Am J Med Genet* **107**, 317–324.

Szabo-Rogers HL, Geetha-Loganathan P, Nimmagadda S, et al. (2008) FGF signals from the nasal pit are necessary for normal facial morphogenesis. *Dev Biol* **318**, 289–302.

Wang Y, Xiao R, Yang F, et al. (2005) Abnormalities in cartilage and bone development in the Apert syndrome FGFR2(+/S252W) mouse. *Development* **132**, 3537–3548.

Yin L, Du X, Li C, et al. (2008) A Pro253Arg mutation in fibroblast growth factor receptor 2 (Fgfr2) causes skeleton malformation mimicking human Apert syndrome by affecting both chondrogenesis and osteogenesis. *Bone* **42**, 631–643.